



Microstructure and Mechanical Properties of Ni-based Superalloy K418 Produced by the Continuous Unidirectional Solidification Process

Fan Yang, Jiang Wang, Jianbo Yu, Zhenghua Zhou, Baojun Wang, Tingsheng Tu, Xingfu Ren, Kang Deng, and Zhongming Ren

(Submitted February 19, 2019; in revised form August 26, 2019; published online October 17, 2019)

Adopting effective strategies to control the solidification structure of Ni-based superalloys is a very interesting subject for metallurgists. Despite the achievement of developing and applying the continuous unidirectional solidification process in simple alloys, the utilization of this process for K418 alloys has been ignored. The microstructure and mechanical properties of a K418 alloy ingot produced by the continuous unidirectional solidification process were investigated. We found that the γ dendrites were typically cross-shaped in the transverse section. The orientation of surviving grains along the casting direction was $\langle 001 \rangle$ during competitive growth. The secondary dendrite arm spacing was $32.3 \pm 2.5 \mu\text{m}$ at a cooling rate of $1.75 \pm 0.35 \text{ }^\circ\text{C/s}$ from the surface to the center of the K418 alloy ingot. Due to the higher cooling rate than that of the conventional casting process, a more uniform microstructure and finer γ' precipitation were obtained in the ingot. Thus, compared with the conventional casting, the tensile strength and the elongation are increased by 8.4 and 21.3%, respectively, at 25 $^\circ\text{C}$. The tensile strength and elongation increased by 15.2 and 49.3%, respectively, at 800 $^\circ\text{C}$. In addition, the fracture surfaces exhibited numerous typical dimples and dendritic fracture characteristics.

Keywords continuous unidirectional solidification process, K418 alloy, mechanical properties, microstructure

1. Introduction

The Ni-based superalloy K418 is widely used as a component of turbine blades due to its good mechanical properties and excellent hot corrosion resistance. The improvement in the casting of Ni-based superalloys not only is a function of composition but also is associated with their manufacturing process, such as vacuum induction melting (VIM), electroslag remelting (ESR), vacuum arc remelting (VAR), double (VIM + VAR) melting, triple (VIM + ESR + VAR) melting, and vacuum-electromagnetic casting. A major breakthrough concerning the casting Ni-based superalloys occurred in the 1950s with the VIM and refining processes. The normal process of Ni-based superalloys was VIM and conventional casting into master alloy ingots. Then, the master alloy ingots were vacuum remelted and cast into final products (Ref 1). There were quality problems with master alloy ingots made by the conventional casting process, such as nonmetallic

inclusions, coarse grains, shrinkage porosity, and substantial segregation. There was also a large amount of scrap material from the numerous cutoffs, ingot ends, and runner system scrap. Adjusting the melting process could lead to significantly improved quality. High-purity ingots have been obtained by the ESR process with low-frequency alternating current and a transverse magnetic field (Ref 2). The quality of the ingots is determined by the time-variation and asymmetric distribution of the arc during VAR hinder slag discharge by the molten pool (Ref 3). The quantity and average size of inclusions are reduced by double-melting and triple-melting processes. Hence, triple-melting generates fewer and smaller inclusions than those of the double-melting process (Ref 4). However, there are drawbacks to these processes, such as high energy consumption, time-consuming processes, and high production costs. The increased proportion and reduced size of the equiaxed grains in the K417 superalloy ingot were obtained through the linear electromagnetic stirring (Ref 5). The ratio of central shrinkage decreased from 54 to 34% resulting in an increased material yield from the K417 superalloy ingot.

Compared with the conventional casting process, the main advantages of the continuous casting process are increased productivity and quality and reduced production costs. A number of studies have been conducted to produce Ni-based superalloy master alloy ingots by the continuous casting process. The continuous casting parameters, especially the alternative drawing mode, had a great effect on the local solidification condition (Ref 6, 7). The continuous casting process could be a viable method for industrial production of Inconel 713C. Furthermore, an 8 t vacuum horizontal continuous casting (VHCC) production line of Ni-based superalloy was built by the Ross and Catherall company (Ref 8). There is no detailed report of the continuous casting parameters of this production line. The significantly reduced depth of the oscillation mark and quantity of the TiN inclusions of Incoloy

Fan Yang, Jiang Wang, Jianbo Yu, Zhenghua Zhou, Baojun Wang, Tingsheng Tu, Xingfu Ren, Kang Deng, and Zhongming Ren, State Key Laboratory of Advanced Special Steel and Shanghai Key Laboratory of Advanced Ferrometallurgy and School of Materials Science and Engineering, Shanghai University, Shanghai 200072, People's Republic of China. Contact e-mails: fanyang605819@163.com, jiangwang@i.shu.edu.cn, jbyu@shu.edu.cn, 15801978872@163.com, csu-me@163.com, tstu@shu.edu.cn, renxingfu888@163.com, dengk2000@163.com, and renzm2201@163.com.

800H superalloy billets were obtained by electromagnetic continuous casting (Ref 9). Due to characteristics of the VHCC process such as bottom casting and rapid solidification by a water-cooled copper mold, the cleanliness and mechanical properties of the K418 alloy ingots ($\Phi 32$ mm) were improved (Ref 10). However, there may be central segregation and other surface defects, such as segregation tumors, and cracks.

To avoid the defects that occur during the continuous casting process, a new process named continuous unidirectional solidification was developed. There are two styles of the continuous unidirectional solidification process: the Ohno continuous casting (OCC) (Ref 11) and the heating-cooling combined mold (HCCM) approaches (Ref 12). Due to the solidification characteristics of the continuous unidirectional solidification process, the columnar structure and even a single grain structure along the ingot can be produced. The direction of unidirectional Al-CuAl₂ eutectic produced by the OCC process was parallel to the casting direction, and the primary dendrite arm spacing was refined to 100 nm. The mechanical properties were much higher than those of the conventional casting process (Ref 13). Due to the liquid-solid interface located at the outlet of the mold, there tended to be breakout accidents when the casting speed was fast. The HCCM process not only solved the breakout problem but also increased the casting speed of the OCC process (Ref 14). Despite the progressed achievement in applying the continuous unidirectional solidification process to low melting point metals and simple alloys, the utilization of this process on the Ni-based superalloy K418 alloy has been ignored.

In this work, we explored the continuous unidirectional solidification process for the production of K418 alloy ingots. The effects of this process on the microstructure and mechanical properties of K418 alloy ingot were investigated. In addition, the causes of microstructure changes and fracture mechanisms are discussed.

2. Experimental Equipment and Procedures

The typical chemical composition of the K418 alloy is given in Table 1. The liquidus and solidus temperatures of the K418 alloy are 1345 and 1297 °C, respectively, with a solidification range (ΔT) of 48 °C (Ref 15).

Figure 1 shows a schematic illustration of the continuous unidirectional solidification process equipment, including the heating system, cooling system, and traction system. The heating system included an electric furnace and an alumina crucible with an inner diameter of 20 mm and a length of 100 mm. The cooling system included a boron nitride mold with an inner diameter of 10 mm and a length of 100 mm and a water-cooled sleeve with a cooling water volume of 1.8 L/min. The mold was composed of boron nitride due to its good thermal stability, excellent lubricity and machinability, and

Table 1 Typical chemical composition of the K418 alloy (wt.%)

Cr	Mo	Nb	Al	Ti	Zr	C	B	Ni
12.4	3.8	1.8	5.5	1.0	0.11	0.12	0.01	Bal.

absence of a reaction with the K418 alloy melt. The alumina crucible and nitride mold were connected together by a graphite pipe with an inner diameter of 16 mm and a length of 80 mm. The traction system included a dummy rod and a withdrawal device. The dummy rod was injected into the boron nitride mold before heating to a distance of 60 mm.

The K418 alloy master ingots were prepared by VIM and casting the melt into steel molds ($\Phi 80$ mm) under a vacuum atmosphere. The K418 alloy ingot was sectioned into small pieces with a size of $\Phi 15 \times 80$ mm. A small piece of the K418 alloy was heated to 1540 °C at a speed of 7.5 °C/min, and the melt was maintained at 1540 °C for 15 min under argon gas. When the melt flowed into the mold and contacted the dummy rod, it solidified immediately due to the cooling of the dummy rod. The K418 alloy ingot was drawn out by a withdrawal device and an alternating drawing-stopping mode. The parameters of the continuous unidirectional solidification process are given in Table 2.

To record the local temperature evolution during the continuous unidirectional solidification process, a thermocouple was injected into the entrance of the boron nitride mold. A cooling curve was obtained from the measured data as shown in

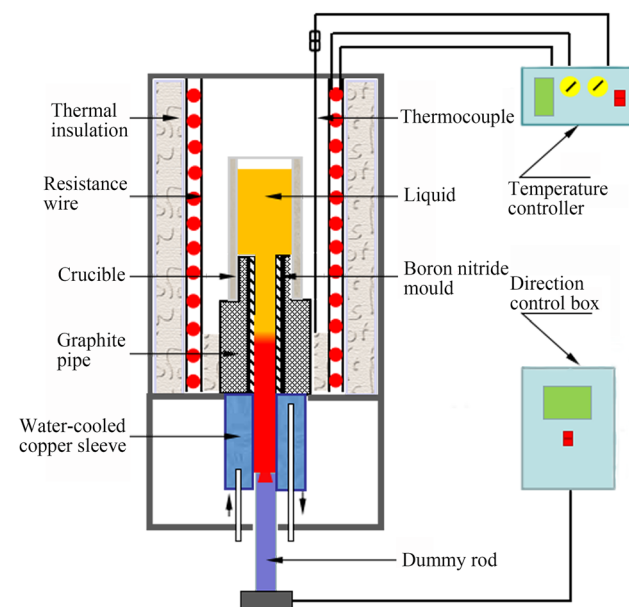


Fig. 1 Schematic illustration of the continuous unidirectional solidification process equipment

Table 2 Parameters of the continuous unidirectional solidification process

Parameters	Unit	Value
Withdrawal length	mm	3
Duration of drawing stroke	s	2
Pause time	s	8
Withdrawal speed	mm/s	1.5
Casting temperature	°C	1540
Water flowing rate	L/min	1.8
Inlet water temperature	°C	24
Outlet water temperature	°C	25

Fig. 2. A cooling rate (\dot{T}) of 2.2 °C/s was measured at the solidification front. The specimens for observing the microstructure and mechanical properties were taken from the steady-state growth region by wire electrodischarge machining, as shown in Fig. 3.

The microstructures were observed using optical microscopy (OM, Leica DM 6000 M) after grinding, polishing, and etching with a solution of 4 g CuSO₄ + 20 mL HCl + 20 mL H₂O. The secondary dendrite arm spacing (λ_2) was measured based on the line-intercept method (Ref 16) and carried out at 30 different sites on the longitudinal sections. The morphology of the γ' precipitate was examined by scanning electron microscopy (SEM, FEI Quanta 450). The concentrations of the alloying elements in the dendrite arm and interdendritic region were measured by energy-dispersive spectroscopy (EDS Octane Plus) operating at 25 kV. To enhance reliability, the EDS was performed at 10 different sites on the transverse section. The sampling time for each point was set at 30 s. The software TEAM was used to determine the fractions of each alloying element at each measured location. Electron backscattering diffraction (EBSD) measurements were also taken using an Apollo 300 SEM microscope equipped with an Oxford Nordlys detector. The recording and indexing of the pseudo-Kikuchi lines were performed with the software Channel5. Finally, the total length and gauge length of the tensile bars were 60 mm and $\Phi 5 \times 25$ mm, respectively, which were measured by a Vernier caliper with an accuracy of 0.01 mm. The tensile bars were then ground with #400, #600, #800, #1200, and #2000 grit silicon carbide papers to remove the surface machining defects. To enhance the reliability and accuracy of this work, three tensile tests were performed at 25 °C and 800 °C. The tensile test was performed on a DNS100 universal test machine at a strain rate of 0.06 mm/min, and the average value was calculated and used in this work. In

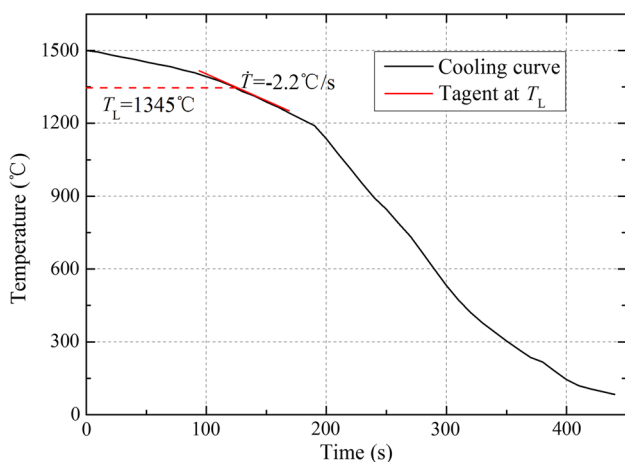


Fig. 2 Cooling curve of the K418 alloy ingot produced by the continuous unidirectional solidification process

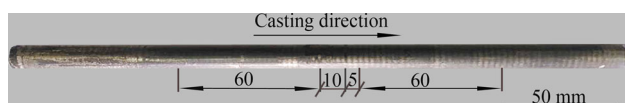


Fig. 3 Positions of the sectioned specimens of the K418 alloy ingot

addition, the morphologies of the fraction surfaces were also observed by SEM.

3. Results and Discussion

3.1 Microstructures

Figure 4 shows that the γ dendrites in the K418 alloy ingot produced by the continuous unidirectional solidification process were typically cross-shaped and evenly distributed along the transverse section. The longitudinal axis of the dendrites was parallel to the casting direction on the longitudinal section, which is similar to the typical microstructure produced by directional solidification. The long and parallel dendritic structure was caused by the temperature gradient along the longitudinal axis direction of the ingot during the continuous unidirectional solidification process.

The results of λ_2 measured at different positions on the longitudinal section are shown in Fig. 5. According to the relationship between λ_2 and the local solidification time (t_f) of the Inconel 713C (Ref 17):

$$\lambda_2 = At_f^n = A (\Delta T / \dot{T})^n \quad (\text{Eq 1})$$

where $A = 6.79 \times 10^{-6} \text{ m/s}^n$ and $n = 0.43$. The λ_2 and \dot{T} of different casting conditions are shown in Fig. 6. The value of the λ_2 slightly decreased from 34.1 to 30.5 μm , and \dot{T} slightly increased from 1.5 to 2 °C/s from the surface to the center of the ingot, respectively. The calculated \dot{T} was consistent with that obtained by the cooling curve. The value of the λ_2 gradually increased from 4.5 to 10.6 μm , and \dot{T} decreased from 169 to 23 °C/s from the surface to the center, respectively, of the continuously cast Inconel 713C ingot with a diameter of 10 mm (Ref 7). Additionally, the λ_2 gradually increased from 64.4 to 78.4 μm , and \dot{T} decreased from 0.26 to 0.16 °C/s from the surface to the center, respectively, of the conventionally cast K418 ingot with a diameter of 80 mm. The results showed that the \dot{T} during the continuous unidirectional solidification process was more uniform and larger than those of the continuous casting and conventional casting processes, respectively. The condition of the heat flow was directly dependent on the style of the mold. There were differences in the heat flow among the three processes. The direction of the thermal gradient was parallel to the casting direction and along the radial direction from the surface to the center of the continuous unidirectional solidification and the other two processes. The solidification microstructures were greatly dependent on the condition of the heat flow (Ref 18). As a consequence, the microstructure of the K418 alloy ingots produced by the continuous unidirectional solidification process was more uniform than the other two processes.

The columnar grains with a $\langle 001 \rangle$ preferred direction grew along the casting direction under the continuous unidirectional solidification process, as shown in Fig. 7(a1) and (a2). The preferred $\langle 001 \rangle$ growth direction of cubic crystals was a result of the anisotropy of the surface energy (Ref 19). The grains tended to grow along the direction perpendicular to the liquid/solid interface, which provided the maximum driving force for solidification (Ref 20). It was easier for grains with a preferred growth direction to grow along the direction of the thermal gradient. Due to the effects between the preferred growth direction and thermal gradient, the orientation of the

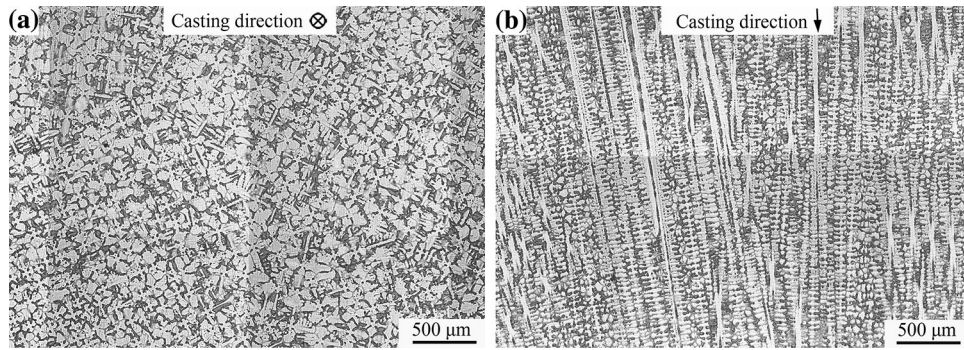


Fig. 4 Microstructures on (a) the transverse and (b) longitudinal sections of the K418 alloy ingot

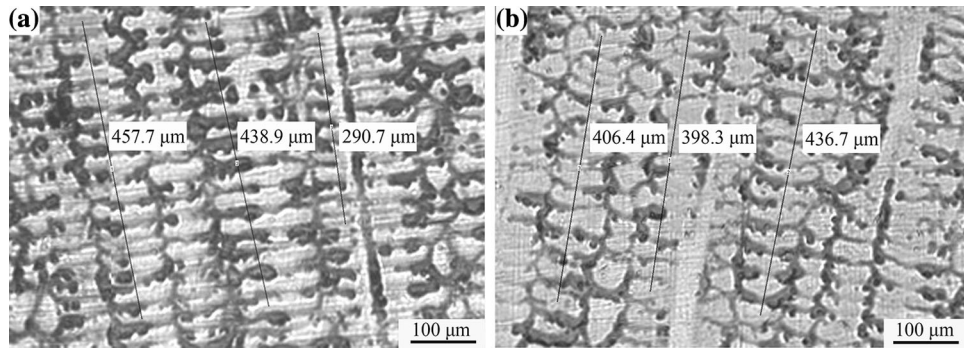


Fig. 5 λ_2 at (a) 5 mm and (b) 0.5 mm from the surface of the K418 alloy ingot

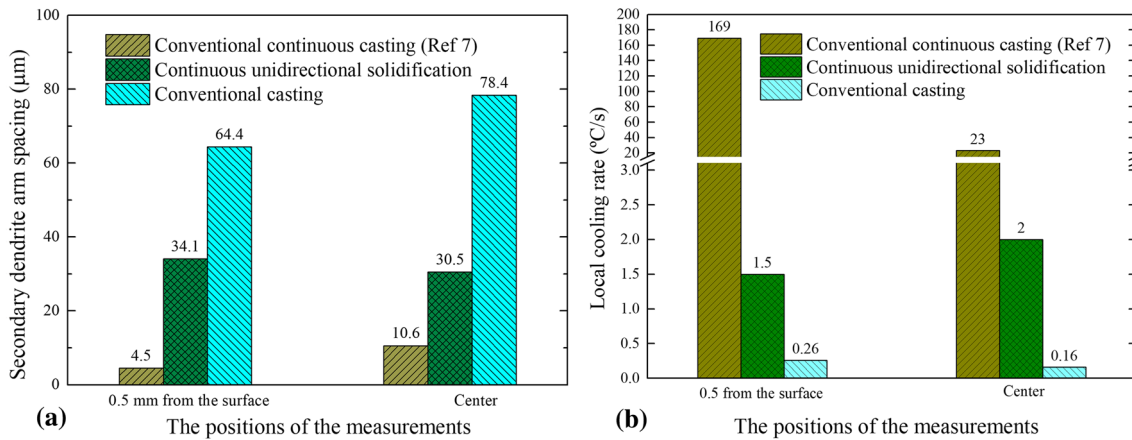


Fig. 6 (a) λ_2 and (b) \dot{T} on the surface and the center under different casting conditions

dominant grains along the casting direction was $\langle 001 \rangle$ as a result of the competitive growth of the K418 ingot produced by the continuous unidirectional solidification process. In addition, the grain orientations were away from the centerline of the K418 alloy ingot as shown in Fig. 7(b1) and (b2). This suggested that the liquid/solid interface was convex with respect to the solidified portion of the ingot. The grain orientations were directly influenced by the curvature of the liquid/solid interface (Ref 21). The greater the deviation of the liquid/solid interface from planarity, the greater the separation of the grain orientations that may occur during the continuous unidirectional solidification process. A planar solidification front generally led to a sharp $\langle 001 \rangle$ texture, and a curved solidification front led to a diffuse texture. The shapes and

positions of the liquid/solid interface were based on the thermal measurements and grain orientations (Ref 22). The position of the convex liquid/solid interface was located in the heating zone during continuous unidirectional solidification due to the elevated inward heat flux on the surface. The distance between the liquid/solid interface and the entrance of the boron nitride mold was 39 mm, as shown in Fig. 2. Consequently, grains angled away from the centerline and the shape of the liquid/solid interface was convex with respect to the solidified portion during the continuous unidirectional solidification process.

The γ' precipitate is the major strengthening phase in the K418 alloy. It precipitated from the supersaturated γ matrix during the solidification process. At a withdrawal speed of

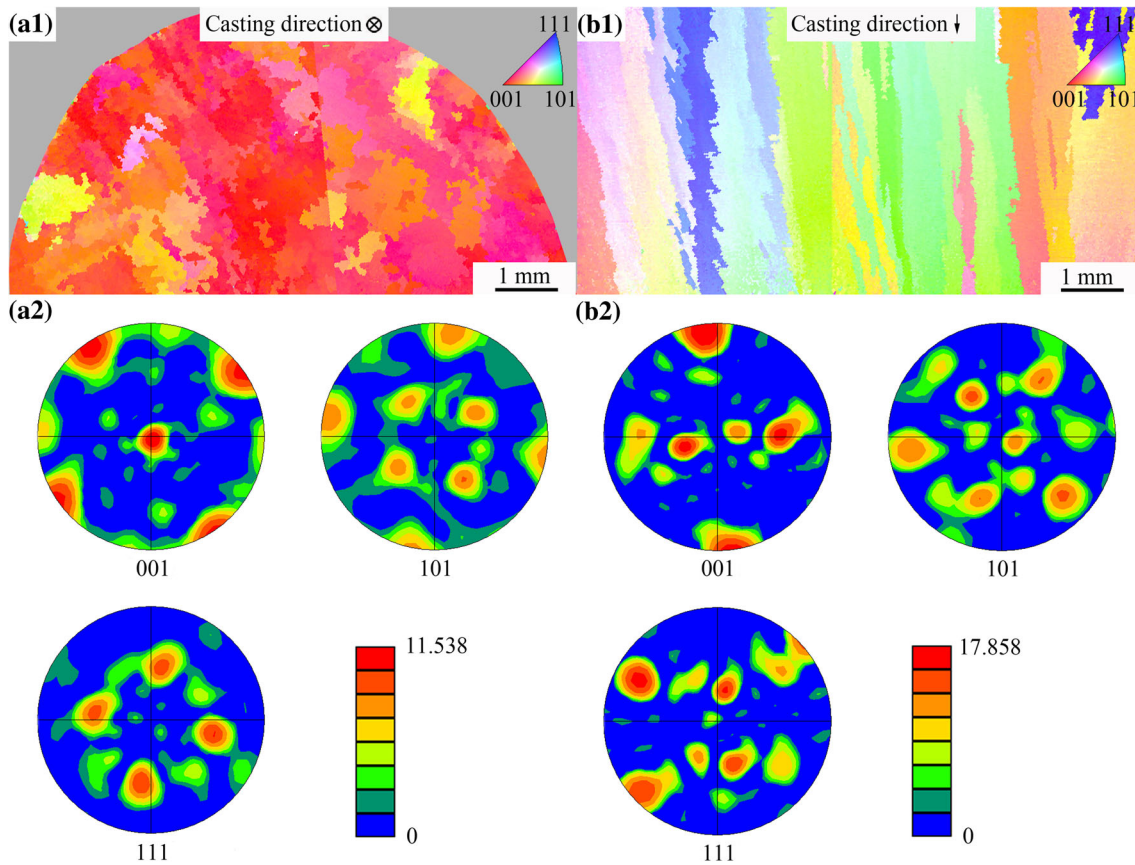


Fig. 7 Orientation maps of (a1) and (a2) the transverse and (b1) and (b2) longitudinal sections of the K418 alloy ingot

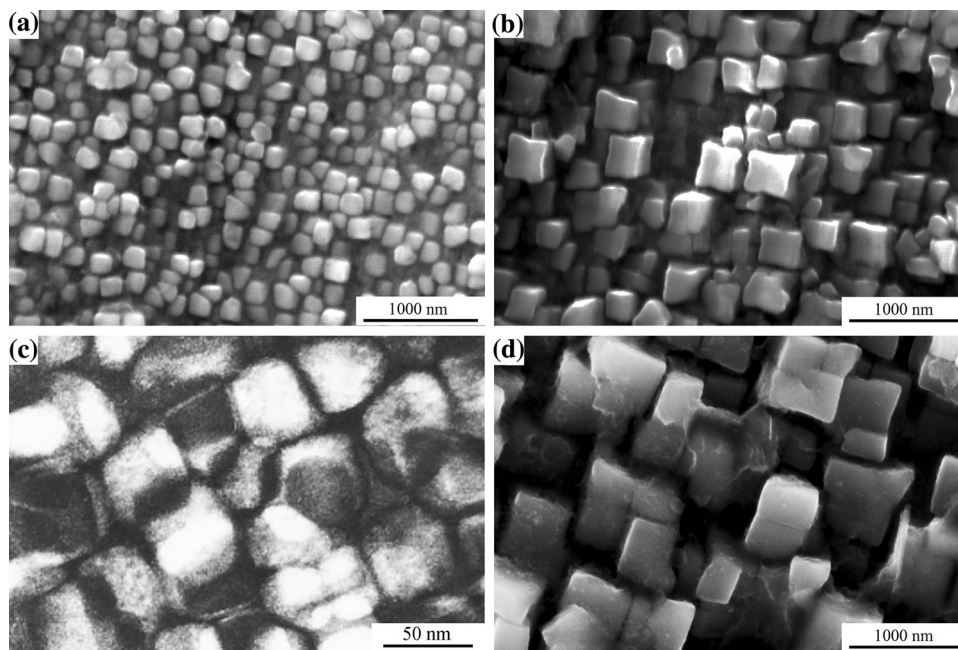


Fig. 8 Morphologies of γ' precipitates in (a) the dendritic arm and (b) interdendritic region of the K418 alloy ingot under different casting conditions: (a) and (b) the continuous unidirectional solidification, (c) the continuous casting (Ref 7), and (d) the conventional casting

300 $\mu\text{m/s}$, the morphologies of the γ' precipitate tended to be spherical in the dendritic arm and spherical-cubic mixture in the interdendritic region, as shown in Fig. 8(a) and (b). The morphologies of the γ' precipitate were cuboid and butterfly-

like shape under the continuous casting and conventional casting conditions, respectively, as shown in Fig. 8(c) and (d). The sizes of the γ' precipitate were 0.17 and 0.26 μm in the dendritic arm and interdendritic region, respectively, which are

bigger than those with a size of 0.06 μm from continuous casting (Ref 7) and smaller than those with a size of 0.78 μm from conventional casting. The morphology of γ' precipitates generally evolves in the sequence of sphere, cube, octocube, and dendrite during coarsening (Ref 23). When the particle size is small, the γ' precipitate is spherical. As the precipitates gradually grow, their shapes change from spherical to cuboid. Cuboid particles with a certain size split into subparticles, such as doublets or octets. The experimental and theoretical studies demonstrated that the shapes of γ' precipitates are determined by the size of the precipitates (Ref 23-25). For isolated precipitates, the theoretical sequence of the morphology evolution is as follows: sphere \rightarrow cube when $L \geq 7.7\delta$, cube \rightarrow doublet when $L \geq 27\delta$, doublet \rightarrow octet when $L \geq 82\delta$, and octet \rightarrow platelet when $L \geq 377\delta$, where L is the edge length of the cube and δ is the ratio of the interfacial free energy to the elastic energy (Ref 25). The driving forces for the γ' precipitate nucleation are the degrees of supercooling and supersaturation (Ref 26). The supercooling of the continuous unidirectional solidification process is increased due to the higher cooling rate than the conventional casting process. It not only promoted the rate of nucleation but also reduced the growth time of the γ' precipitates. Therefore, the refined γ' precipitates in the K418 alloy ingot were obtained by the continuous unidirectional solidification process.

The averages and standard deviations of the EDS quantity analyses in the dendritic arm and the interdendritic region are shown in Table 3. Figure 9 shows the mean EDS quantitative analysis in the dendritic arm and the interdendritic region of the K418 alloy ingot. It was found that Al, Ti, Mo, and Nb segregated to the interdendritic region. Due to the depletion of forming elements and the high cooling rate, the precipitation of the γ' phase did not occur readily in the dendritic arms.

However, the high supersaturation in the interdendritic region was obtained due to the enrichment of the forming elements. The nucleation initiated earlier, and greater growth kinetics occurred for the γ' precipitate in the interdendritic regions than those in the dendritic arms (Ref 27). It was concluded that the size of the γ' precipitate in the interdendritic regions was larger than that in the dendritic arms.

3.2 Mechanical Properties

Figure 10 shows the size and the stress-strain curves at 25 and 800 $^{\circ}\text{C}$ of the K418 alloy tensile bars. Both of the curves exhibited the strain hardening and necking stages at 25 and

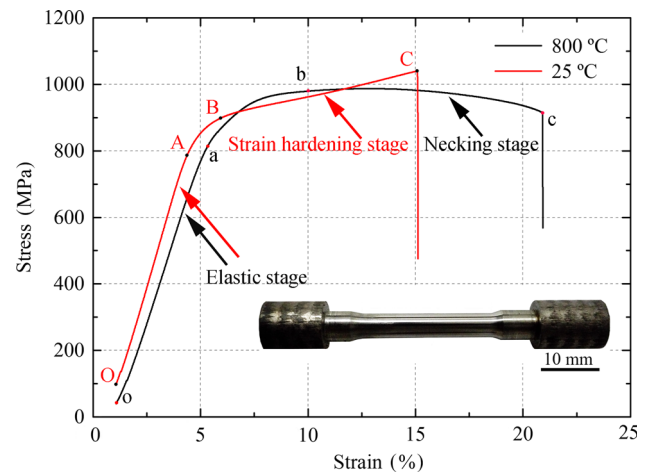


Fig. 10 Size and stress-strain curves at 25 and 800 $^{\circ}\text{C}$ of the K418 tensile bars

Table 3 Averages (μ) and standard deviations (σ) of the EDS quantity analyses in the dendritic arm and the interdendritic region (wt.%)

Positions	Elements									
	Nb		Ti		Mo		Al		Cr	
	μ	σ	μ	σ	μ	σ	μ	σ	μ	σ
Dendritic arm	0.7	0.1	0.9	0.2	2.0	0.1	4.1	0.3	12.3	0.3
Interdendritic region	1.4	0.2	1.2	0.2	2.6	0.5	5.1	0.6	12.9	0.4

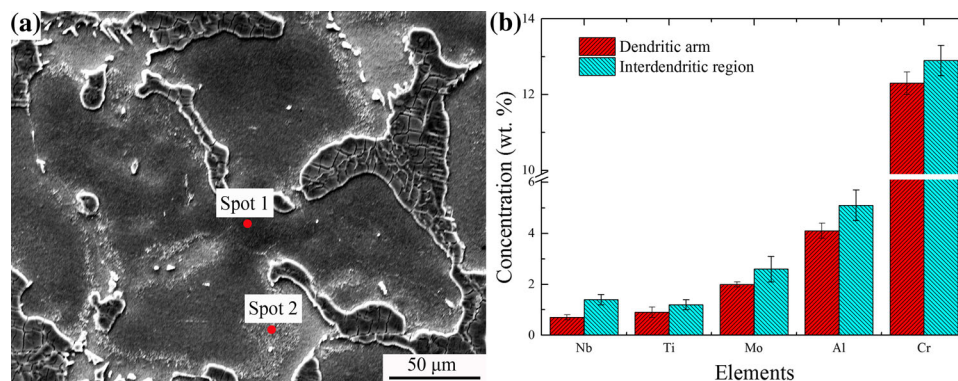


Fig. 9 (a) positions and (b) concentrations from EDS in the dendritic arm and interdendritic region of the K418 alloy ingot

800 °C, respectively. Besides, there was no yield stage at 25 and 800 °C. The plastic deformation of the superalloy is accompanied by the movement of dislocation. The dominant deformation mechanism is shearing of the γ' precipitate by pairs of $a/2 \langle 110 \rangle$ dislocations at low temperature (below 600 °C) and is dislocation climb at high temperature (above 800 °C). Additionally, the two mechanisms are all observed at intermediate temperatures (Ref 28). K418 alloy is mainly strengthened by the γ' precipitate which is the main barriers for dislocation moving. Due to the smaller stress values and larger amount of slip bands for the dislocation climb mechanism at 800 °C than those for the dislocation shear mechanism at 25 °C, the lower tensile strength and higher elongation are obtained at 800 °C, as shown in Fig. 10.

The averages and standard deviations of the tensile properties of this process are shown in Table 4. The mean tensile strength and elongation reached 1014 ± 25 MPa and $9.1 \pm 0.5\%$, respectively, at 25 °C. In addition, the mean tensile strength and elongation reached 991 ± 30 MPa and $11.2 \pm 1.4\%$, respectively, at 800 °C. The mean mechanical properties of the K418 alloy ingots under different casting conditions are given in Fig. 11. Compared with the conventional casting, the tensile strength and the elongation increased by 8.4 and 21.3%, respectively, at 25 °C. Additionally, the tensile strength and elongation increased by 15.2 and 49.3%, respectively, at 800 °C. The mechanical properties of the continuous unidirectional solidification specimens were better than those from conventional casting (Ref 10). The improvements in the mechanical properties were caused by the uniform microstructure, refined γ' precipitate, and the columnar grains without radial grain boundary along the casting direction.

Table 4 Averages (μ) and standard deviations (σ) of the tensile strengths (Rm) and elongations (A) at 25 and 800 °C

Sample	Property			
	25 °C		800 °C	
	Rm, MPa	A, %	Rm, MPa	A, %
1	1040	9.2	987	12.7
2	1013	9.5	1023	10.8
3	990	8.5	964	10.1
μ	1014	9.1	991	11.2
σ	25	0.5	30	1.4

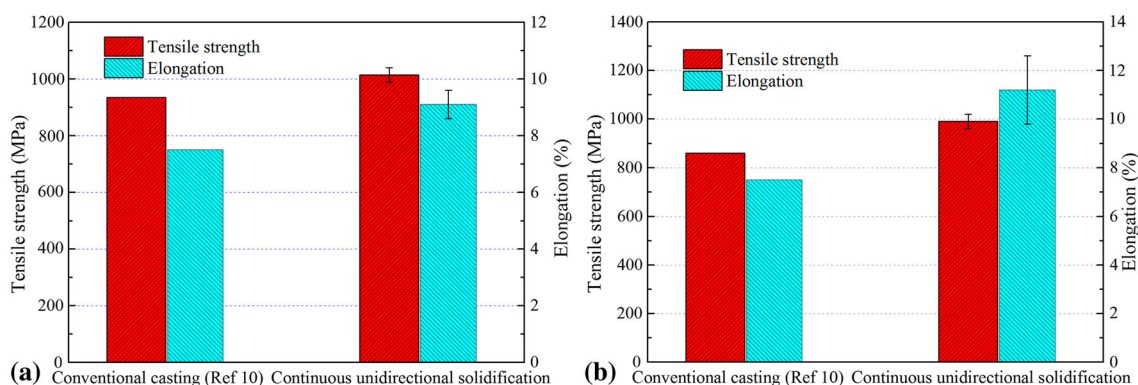


Fig. 11 Mechanical properties at (a) 25 °C and (b) 800 °C of the K418 alloy ingot under different casting conditions

Figure 12 shows the transgranular fracture features at 25 °C (a1, b1, c1, d1) and 800 °C (a2, b2, c2, d2) of the K418 alloy ingot produced by the continuous unidirectional solidification process. The fracture surfaces contained numerous dimples and dendritic fracture features. The fracture mechanism of the K418 alloy ingot was a mixed rupture that contained the numerous typical dimples and dendritic fracture characteristics. Additionally, there was no porosity on the fracture surface due to the dense and uniform microstructure of the K418 alloy ingot, as shown in Fig. 12(a1) and (a2). There were also tearing ridges, dimples, secondary cracks, and shear lips on the fracture surface at both test temperatures. Figure 12(a1) and (a2) shows that the angles between the shear lips and pulling axis were 90° and 45° at 25 and 800 °C, respectively. The 45° shear lip was caused by a tearing break that occurred in the plane stress state. There was a larger shear lip area and secondary cracks with a longer length on the fracture surface at 800 °C than those on the fracture surface at 25 °C, which resulted in the lower tensile strength at 800 °C. There were a greater number of dimples and tearing ridges on the fracture surface at 800 °C than those on the fracture surface at 25 °C, which resulted in better elongation at 800 °C.

4. Conclusions

The Ni-based K418 superalloy ingots produced by the continuous unidirectional solidification process were investigated. The following conclusions can be drawn from this study.

1. The γ dendrites were typically cross-shaped on the transverse section. The longitudinal axis of the dendrites was parallel to the casting direction on the longitudinal section.
2. At a 1540 °C casting temperature, 18 mm/min mean withdrawal speed, and 1.8 L/min cooling water flow rate, the mean secondary dendrite arm spacing was 32.3 ± 2.5 μm , and the cooling rate was 1.75 ± 0.35 °C/s from the surface to the center of the K418 alloy ingots. A uniform microstructure and refined γ' phase were obtained in the K418 alloy ingots by the continuous unidirectional solidification process.
3. Compared with the conventional casting, the tensile strength and the elongation increased by 8.4 and 21.3%, respectively, at 25 °C. Additionally, the tensile strength and elongation increased by 15.2 and 49.3%, respectively, at 800 °C.

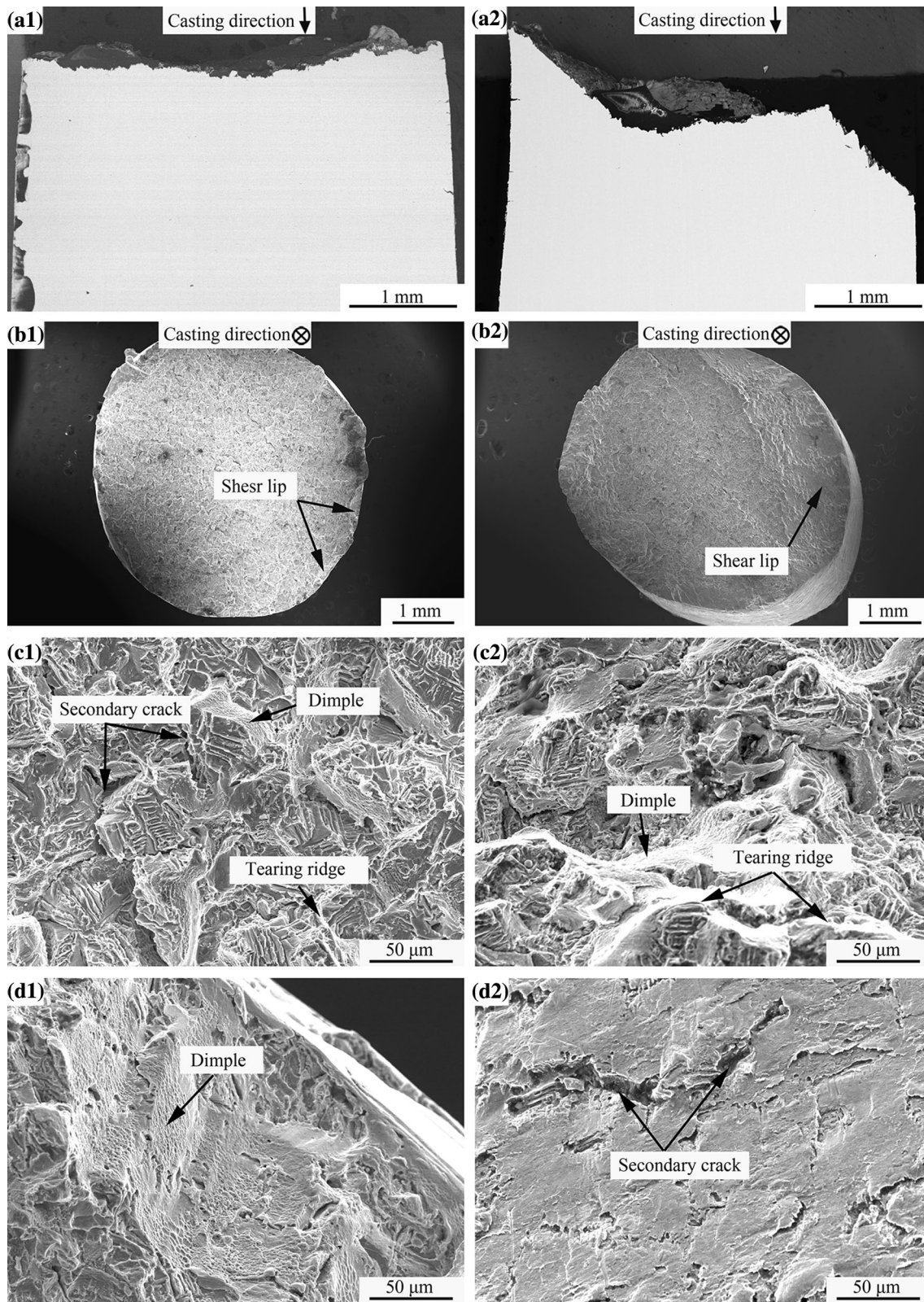


Fig. 12 Images of the fracture surfaces at (a1, b1, c1, d1) 25 °C and (a2, b2, c2, d2) 800 °C of the K418 alloy ingots: (a1) and (a2) longitudinal section, (b1) and (b2) transverse section (c1) and (c2) radiation area, and (d1) and (d2) shear lip

tively, at 800 °C. The improvements in mechanical properties were caused by a uniform microstructure, refined γ' precipitates, and columnar grains without radial grain boundaries along the casting direction.

4. The fracture surfaces exhibited numerous typical dimples and dendritic fracture characteristics. The tensile strength was lower, and the elongation was better at 800 °C than those at 25 °C.

Acknowledgments

This work is financially supported by the Natural Science Foundation of China (Nos. U1560202, 51604171, 51690162), National Science and Technology Major Project “Aeroengine and Gas Turbine” (2017-VII-0008-0102), and the Project of the Ministry of Science and Technology of China (2017YFB0405902).

References

1. J.R. Davis, *Metallurgy, Processing and Properties of Superalloys, Heat-Resistant Materials-ASM Specialty Handbook*, ASM International, Material Park (OH), 1997, p 221–254
2. H. Wang, Y.B. Zhong, Q. Li, Y.P. Fang, W.L. Ren, Z.S. Lei, and Z.M. Ren, Effect of Current Frequency on Droplet Evolution during Magnetic-Field-Controlled Electroslag Remelting Process Via Visualization Method, *Metall. Mater. Trans. B*, 2017, **48**, p 655–663
3. D.M. Shevchenko and R.M. Ward, Liquid Metal Pool Behavior during the Vacuum Arc Remelting of Inconel 718, *Mater. Trans. B*, 2009, **40**, p 263–270
4. Z.Y. Chen, S.F. Yang, J.L. Qu, J.S. Li, A.P. Dong, Y. Gu, Effect of Different Melting Technologies on the Purity of Superalloy GH4738, *Mater.*, 2018, **11**, p 1838–1848
5. W.Z. Jin, J. Li, T.J. Li, and G.M. Yin, Linear Electromagnetic Stirring and Microstructures of K417 Superalloy Master Alloy Ingot, *Chin. J. Vac. Sci. Technol.*, 2008, **28**, p 579–583
6. F. Zupanič, T. Bončina, A. Križman, and F.D. Tichelaar, Structure of Continuously Cast Ni-Based Superalloy Inconel 713C, *J. Alloys Compd.*, 2001, **329**, p 290–297
7. F. Zupanič, T. Bončina, A. Križman, and F.D. Tichelaar, Microstructural Evolution on Continuous Casting of Nickel Based Superalloy Inconel 713C, *Mater. Sci. Technol.*, 2002, **18**, p 811–819
8. D. Hendley, N. Gravill, and C.R. Thomas, Continuously Cast Superalloy Barstock, *Foundry Trade J.*, 2000, **9**, p 24
9. F. Wang, L.T. Zhang, A.Y. Deng, X.J. Xu, and E.G. Wang, Continuous Casting of Incoloy800H Superalloy Billet under an Alternating Electromagnetic Field, *Met.*, 2016, **6**, p 2–13
10. H.L. Luo, D. Feng, S.P. Li, X. Cao, and J.T. Wang, Microstructure and Property of High Cleanliness K418 Superalloy by Vacuum Horizontal Continuous Casting, *J. Iron Steel Res.*, 2016, **28**, p 33–37
11. A. Ohno, Continuous Casting of Single Crystal Ingots by the OCC Process, *JOM*, 1986, **38**, p 14–16
12. J.X. Xie, J. Mei, X.H. Liu, X.F. Liu, A Kind of Process and Equipment for Fabricating Cupronickel Pipes with Heating-cooling Combined Mold Casting, Chinese Patent., 2012, Appl. ZL201010501407.4
13. M. Okayasu, S. Takasu, and S. Yoshie, Microstructure and Material Properties of an Al-Cu Alloy Provided by the Ohno Continuous Casting Technique, *J. Mater. Process. Technol.*, 2010, **210**, p 1529–1535
14. J. Mei, X.H. Liu, Y.B. Jiang, S. Chen, and J.X. Xie, Liquid-Solid Interface Control of BFe10-1-1 Cupronickel Alloy Tubes during HCCM Horizontal Continuous Casting and its Effect on the Microstructure and Properties, *Int. J. Miner. Metall. Mater.*, 2013, **20**, p 748–758
15. Z.X. Shi, J.X. Dong, M.C. Zhang, and L. Zheng, Solidification Characteristics and Segregation Behavior of Ni-Based Superalloy K418 for Auto Turbocharge Turbine, *J. Alloys Compd.*, 2013, **571**, p 168–177
16. R.E. Spear and G.R. Gardner, Dendrite Cell Size, *AFS Trans.*, 1963, **71**, p 209–215
17. A.K. Bhambri, T.Z. Kattamis, and J.E. Morral, Cast Microstructure of Inconel 713C and Its Dependence on Solidification Variables, *Metall. Trans. B*, 1975, **6**, p 523–537
18. S. Kou, *Welding Metallurgy*, Wiley, New York, 1987, p 129–177
19. D. Walton and B. Chalmers, The Origin of the Preferred Orientation in the Columnar Zone of Ingots, *Trans. Metal. Soc. Am. Inst. Min. Met. Eng.*, 1959, **215**, p 447–457
20. M. Gäumann and W. Kurz, Why is it So Difficult to Produce an Equiaxed Microstructure during Welding, *Mathematical Modelling of Weld Phenomena*, Vol 4, H. Cerjak, Ed., Institute of Materials, Minerals and Mining, London, 1998, p 125–135
21. N.M. Souza, M.G. Ardakani, M. Mclean, B.A. Shollock, Directional and Single-Crystal Solidification of Ni-Based Superalloys: Part I. The Role of Curved Isotherms on Grain Selection, *Metall. Mater. Trans. A.*, 2000, **31**, p 2877–2886
22. A.J. Elliott, S. Tin, W.T. King, S.C. Huang, M.F.X. Gigliotti, and T.M. Pollock, Directional Solidification of Large Superalloy Castings with Radiation and Liquid-Metal Cooling: A Comparative Assessment, *Metall. Mater. Trans. A*, 2004, **35A**, p 3221–3231
23. R. Ricks, A. Porter, and R. Ecob, The Growth of γ' Precipitates in Nickel-Base Superalloys, *Acta Metall.*, 1983, **31**, p 43–53
24. T. Miyazaki, K. Nakamura, H. Mori, Experimental and Theoretical Investigations on Morphological Changes of γ' Precipitates in Ni-Al Single Crystals during Uniaxial Stress-Annealing, *J. Mater. Sci.*, 1979, p 1827–1837
25. A.G. Khachaturyan, S.V. Semenovskaya, and J.W. Morris, Theoretical Analysis of Strain-Induced Shape Changes in Cubic Precipitates during Coarsening, *Acta Metall.*, 1988, **36**, p 1563–1572
26. F. Wang, D. Ma, J. Zhang, L. Liu, J. Hong, S. Bogner, and A. Bührig-Polaczek, Effect of Solidification Parameters on the Microstructure of Superalloy CMSX-6 Formed during the Downward Directional Solidification Process, *J. Cryst. Growth*, 2014, **389**, p 47–54
27. X.P. Guo, H.Z. Fu, and J.H. Sun, Influence of Solid/Liquid Interfaces on the Microstructure and Stress-Rupture Life of the Single-Crystal Nickel-Base Superalloy NASAIR 100, *Metall. Mater. Trans. A*, 1997, **28**, p 997–1009
28. Z.K. Chu, J.J. Yu, X.F. Sun, H.R. Guan, and Z.Q. Hu, Tensile Properties and Deformation Behaviors of a Directionally Solidified Ni-Base Superalloy, *Mater. Sci. Eng. A*, 2010, **527**, p 3010–3014

Publisher's Note Springer Nature remains neutral with regard to jurisdictional claims in published maps and institutional affiliations.